

CHAPTER 1
Introduction

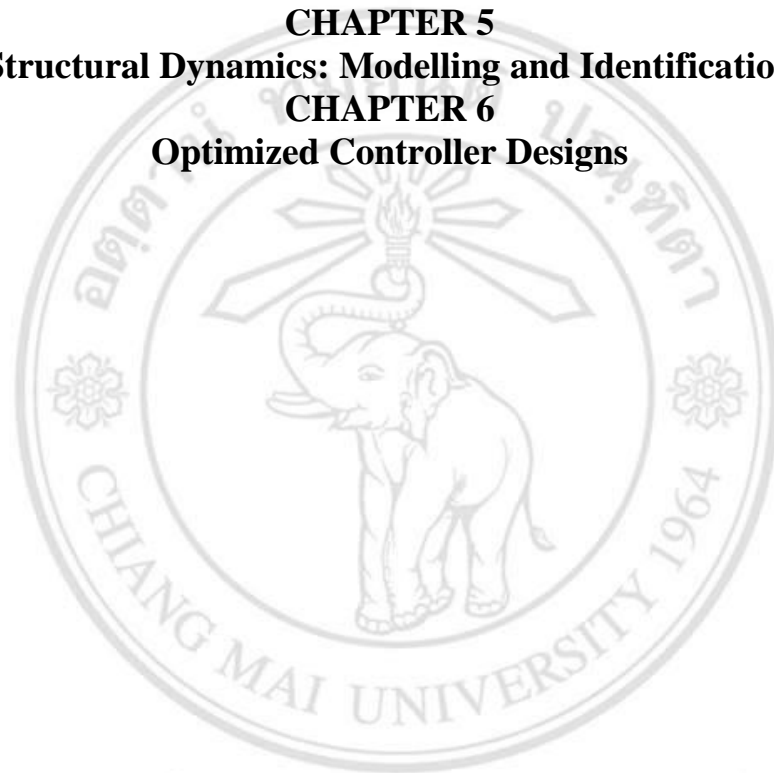
CHAPTER 2
Machining Dynamics

CHAPTER 3
Robust Control Approach

CHAPTER 4
Hardware-in-the-Loop Test System for Machining Emulation

CHAPTER 5
Structural Dynamics: Modelling and Identification

CHAPTER 6
Optimized Controller Designs



ลิขสิทธิ์มหาวิทยาลัยเชียงใหม่
Copyright© by Chiang Mai University
All rights reserved

CHAPTER 7

Optimized Controller Performance

In this chapter, both numerical and experimental results are reported for the controller designs described in Chapter 6. The results are based on two different versions of the system models:

M1: reduced order FE model (5.4)

M2: system ID reduced order model with 4 states (5.20).

The fundamental data for the test system structure and the models can be also seen in Figure 5.11 for FE model, Figure 5.12, system ID model and in Figure 5.13 which compares the FE model and system ID models.

7.1 Closed-Loop Behaviour without Cutting

The synthesis of the controller solutions was undertaken using the LMI control synthesis routines within the MATLAB® program. The controller designs presented in Chapter 6 can be considered in four groups:

- 1) State feedback controllers via LKF for time-delay system model with 3 different optimization cases, SFC1, SFC2 and SFC3.
- 2) State feedback controller based on robust LQR solution.
- 3) Output feedback controllers via LKF for time-delay system model.
- 4) Output feedback controllers using standard (non-time-delay) robust synthesis methods to account for cutting force effects

7.1.1 State feedback controllers

For the state feedback controllers, the system model has a number of output measurements equal to the number of states (velocities and displacements). The synthesis calculations for these controllers were based on the FE model in (5.14). The state feedback gains for the synthesized controllers are shown in Table 7.1.

The robustness properties of the full state feedback controllers can be evaluated from the complementary sensitivity functions T_{ud} as shown in Figure 7.1. Also shown is the weighting function inverse (with $K_w = 2.99$) which gives a close bound for all four cases. It is remarked that, for all four controllers, designs with reduced weighting (smaller K_w) involved higher state feedback gains and tended to destabilize unmodelled high frequency modes when applied to the experimental system, even without simulation of cutting operation. Hence, the given solutions are regarded as the best practically implementable controllers for each design type.

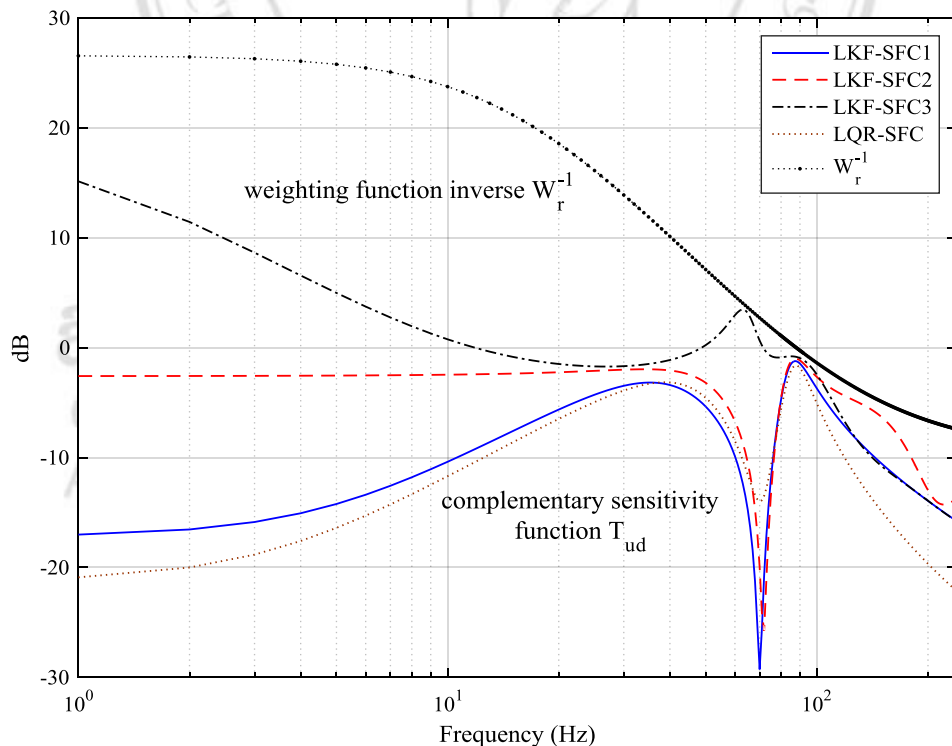


Figure 7.1 Input complementary sensitivity function for optimal controller designs. All controller are seen to satisfy the same robustness criterion, as specified by W_r^{-1}

Table 7.1 State feedback optimal control gain values

	D1	LKF-SFC1	LKF-SFC2		LKF-SFC3		LQR	
	K	K	K	K_r	K (SFC1)	K_r	K	
K_x	K_{x1}	—	-643	-1759	-388	-643	0.064	27.76
	K_{x2}	—	258	1,157	692	258	1,067	-57
	K_{x3}	-19.8	-9.55	-12.7	-2.8	-9.55	0	-3.62
	K_{x4}	—	0.82	0.393	0.087	0.82	0	0.29
K_r	K_{r1}	—	71.7	83.9	18.6	71.7	-0.005	786
	K_{r2}	—	184,324	125,333	27,672	184,324	-5.72	431,444

7.1.2 Output feedback controllers

For output feedback controllers, the results of the robustness properties can also be evaluated from the complementary sensitivity functions T_{ud} as for the state feedback controller case. The results are shown in Figure 7.2 and Figure 7.3.

Note that OFC1 and OFC2 have the designs based on two norm bound constraints. One deals with the model error and the other one deals with time-delay effect of the cutting dynamics. While, for OFC3 and LKF-OFC design, the time-delay effect is accounted for in the system model. We found that the results of T_{ud} for OFC1 and OFC2 (Figure 7.2) are not exceeded the line of Δ_m^{-1} ($\Delta_m^{-1} > T_{ud}$ for all frequency) while for T_{ud} of OFC3 and LKF-OFC (Figure 7.3), there is small cross-overs close to the tool bending frequency.

For all of the controllers, the depth-of-cut parameter b_K is maximized subject to the same design of weighting function W_r for T_{ud} . Under these constraints, the synthesized controllers all achieved stable cutting-free operations.

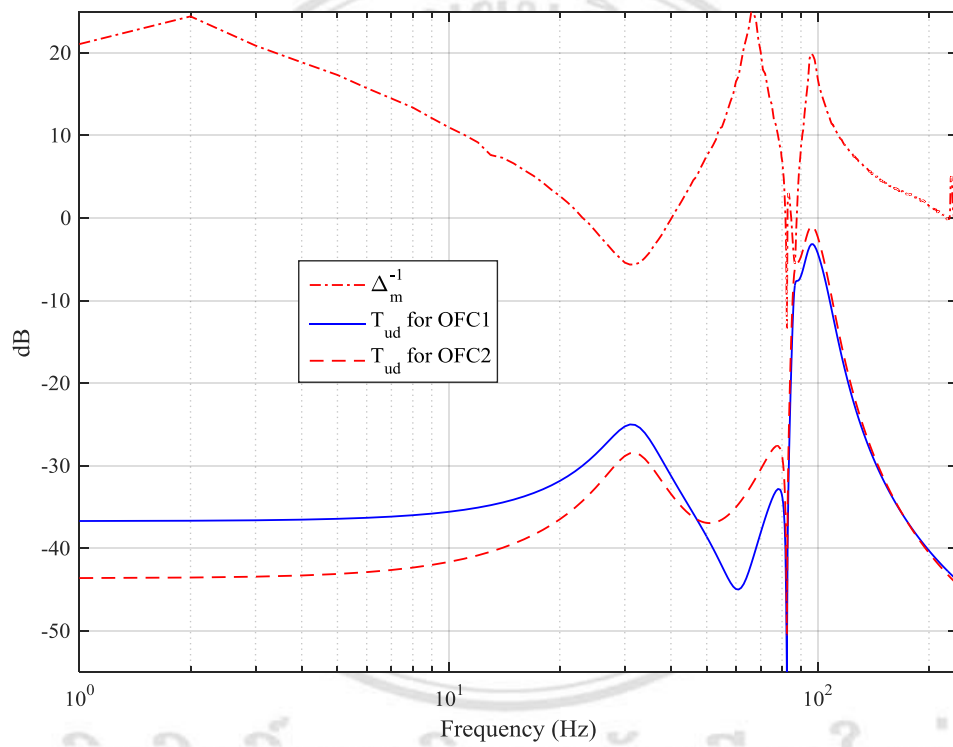


Figure 7.2 Input complementary sensitivity function for optimal controller designs for output feedback controller for OFC1: Dynamics compliance minimization and OFC2: Norm-bounded treatment of delay

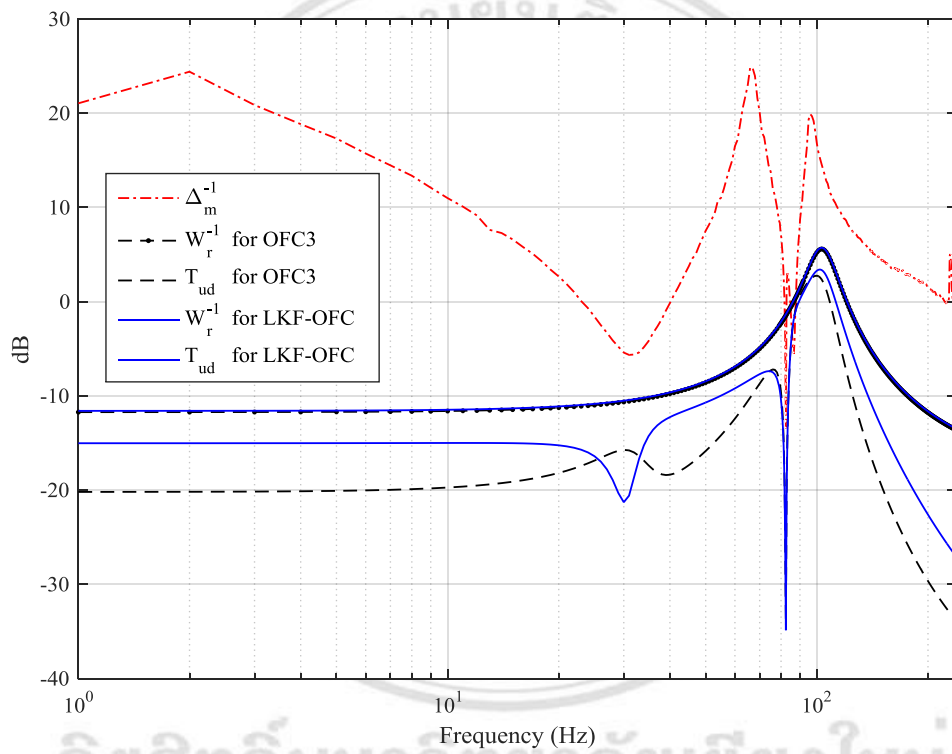


Figure 7.3 Input complementary sensitivity function for optimal controller designs for output feedback controller for OFC3: Padé approximation of delay and the LKF-OFC

7.1.3 Controller implementation

Controllers were implemented using the Real-Time workshop within Simulink and MATLAB® programs as shown in Figure 7.4. The Simulink block diagram for controller implementation includes four main parts: (a) feedback controller, (b) the input/output signal blocks, (c) cutting force model and (d) external excitation signals. Within the controller blocks there are three subsystems which are the local PD controller for a control actuator 1, the PD controller compensating for actuator 2 and the optimally designed controller for which the control signal is superimposed with the PD control signal acting through actuator 1. The displacement and strain signals from the test rig are input to the controller by 16 bit A/D hardware and the control output signals to the actuator amplifiers are through 12 bit D/A hardware. Additional components in the control implementation include display of the I/O signals on target scope (e.g. vibration signals, operating parameters, etc.) and a safety cut-off control switch.

One of the limiting factors for controller operation is the level of noise generated within the control loop. This can be assessed by monitoring the input/output signals when in the idle state, i.e. without cutting forces. The residual noise level for the controller input and output signals as presented in Figure 7.5. The raw noise data is shown in Figure 7.6 for the state feedback controllers and Figure 7.7 for the output feedback controllers. These figures show noise-excited cutting tool displacement vibration y_t and control force u for the test system. We can see that the maximum noise on the control force occurs for OFC2 (norm-bound treatment of delay) and the next highest is OFC1 (dynamic compliance minimization). Over all controllers, we found that the minimum noise levels occur with the LKF output feedback controller and OFC3 (Padé approximation) respectively. The expected noise attenuation properties for the closed-loop system can be evaluated from the frequency response function from additive sensor noise n to the control force u , T_{un} . This frequency response function is shown for the output feedback controllers in Figure 7.8. The values of T_{un} shown for the aforementioned controllers results is in broad agreement with the noise signal measurements.

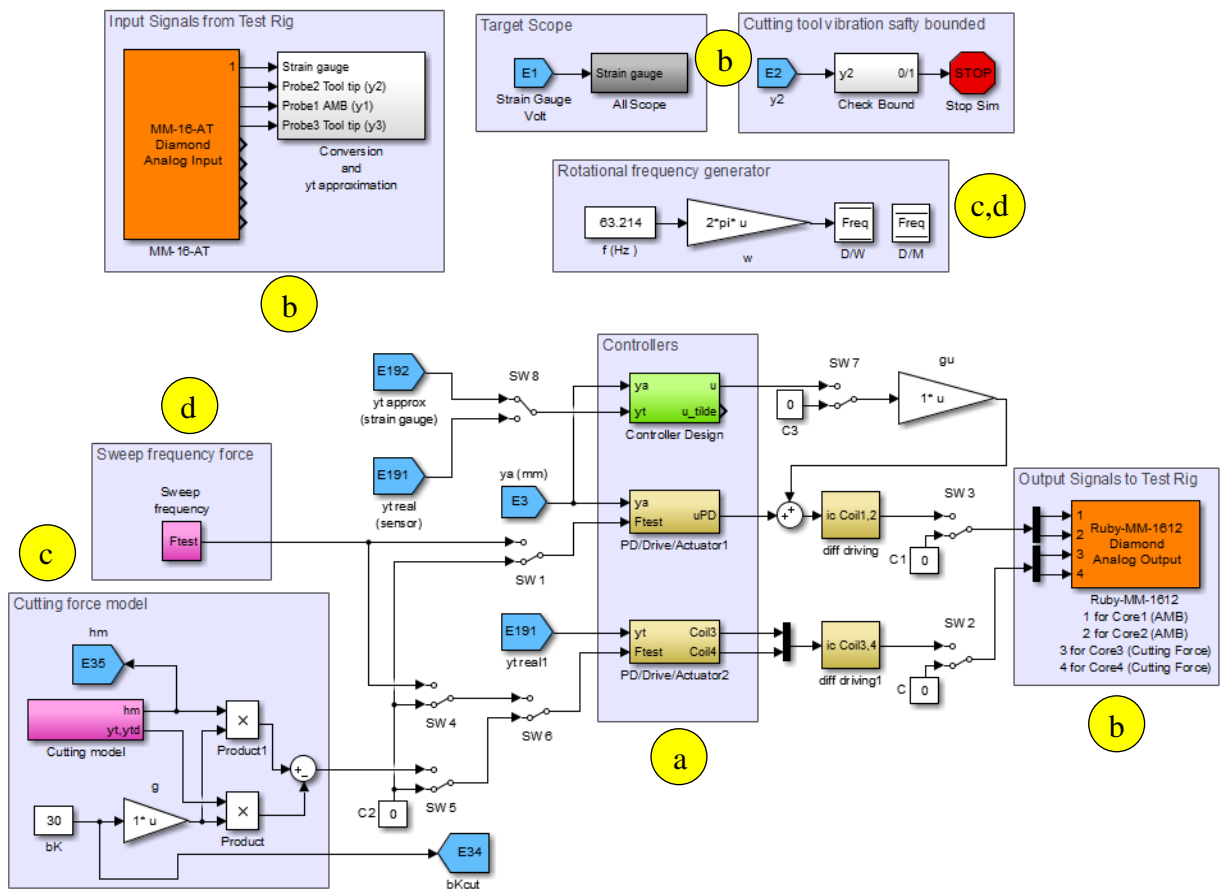


Figure 7.4 Overview of test system control implementation in Simulink

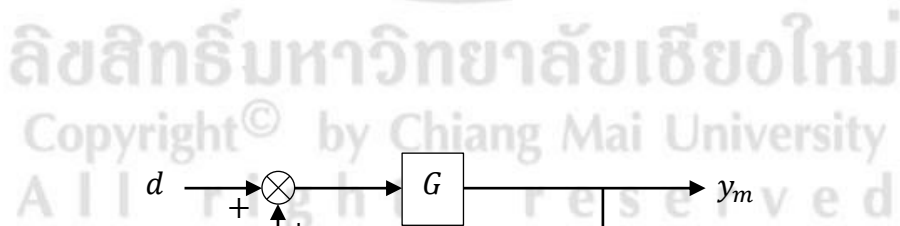


Figure 7.5 Disturbances acting on input/output signals

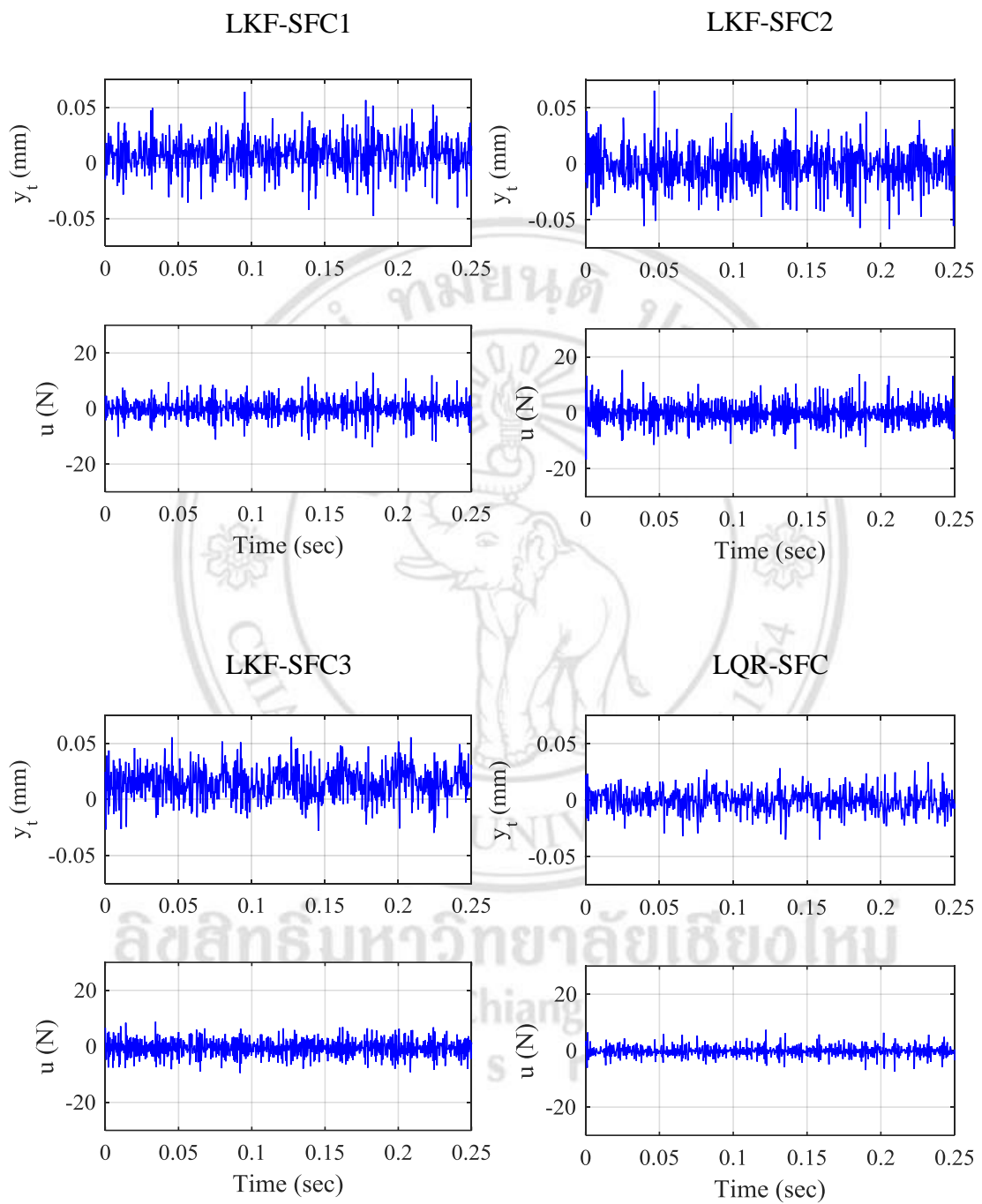


Figure 7.6 Signals induced by noise for different state feedback controllers

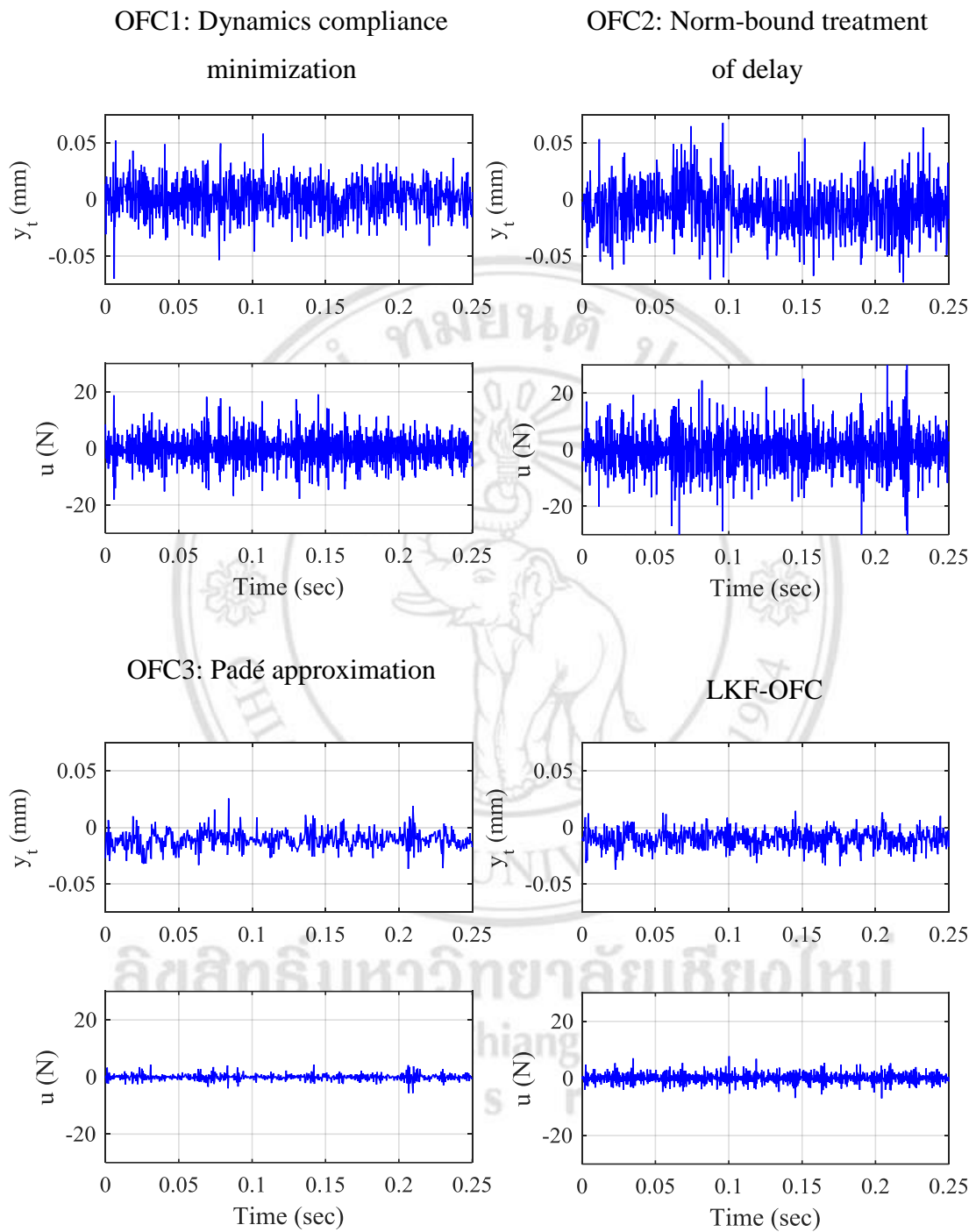


Figure 7.7 Signals induced by noise for different output feedback controllers

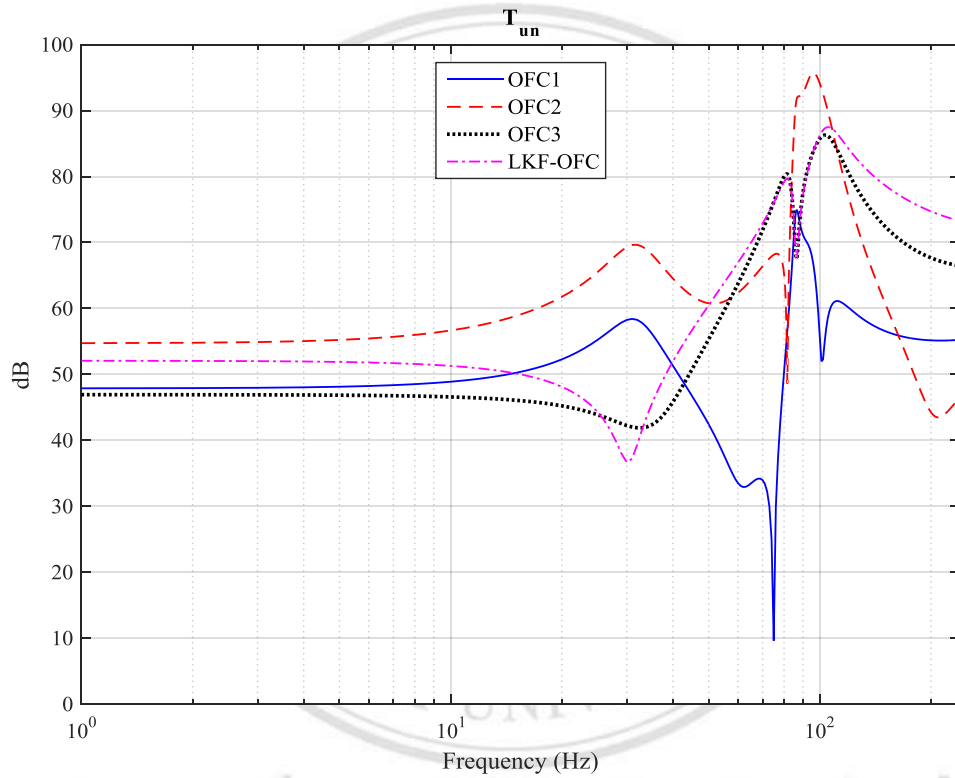


Figure 7.8 Frequency response of the closed-loop system from sensor noise to the system control force T_{un}

7.2 Cutting Stability Boundaries

The experimental results for the cutting stability boundary with local PD controller (Section 4.6) were shown in Figure 4.16. The maximum depth-of-cut parameter was $b_{K,\max} \approx 180$ N/mm. The results for the optimized controllers include eight controller designs (which are applied in parallel control with local PD controller). The procedure for the stability testing is the same as for the local PD controller. The SLD results are shown in Figure 7.9 for state feedback controllers and Figure 7.10 for output feedback controllers. From these graphs, the maximum stable depth-of-cut over all tool rotational frequency $b_{K,\max}$ is found for each controller and can be seen in Table 7.2.

The SLD results for state feedback control confirm that the LKF optimization controller (LKF-SFC1-3) have the best cutting stability boundaries. The maximum cutting stability improvement is achieved with LKF-SFC3. Next, LKF-SFC2 and LKF-SFC1 and LQR-SFC give the least improvement. The state feedback control with delayed feedback gives more improvement than without delayed feedback. Competing lobes can be seen in the SLD for LQR-SFC and LKF-SFC3 associated with the rigid body mode. It can also be seen that the controllers slightly change the natural frequency of the tool bending mode, as indicated by a small shift in the lobe positions on the SLD.

For the output feedback control design without delayed feedback (OFC1-3), the performance improvement depends on how much cutting dynamics is incorporated in the control design synthesis. OFC1 has the least improvement since it completely ignores the cutting dynamics and treats the cutting forces as an unknown disturbance. OFC2 improvement is better than OFC1 since it only ignores the delayed term in the cutting model. OFC3 provides the best result since full model cutting dynamics is considered but the time delay is approximated by Padé approximation. It is worth to mentioning that OFC3 has the lowest noise signal level compared to other output feedback controller designs without delayed feedback (OFC1 and 2).

LKF-OFC achieved the best improvement. For this controller, the full time-delay cutting dynamics were included in the system model so it could be treated as a time-delay system. Since there is no approximation or bounding involved and the controller

has the most general form (with delayed feedback), the optimization achieves the best results and this is reflected in the experimental performance. The stability limit $b_{K,\max}$ is shown in Table 7.2.

Table 7.2 Summary of the stability limits in terms of $b_{K,\max}$ for all controllers

	Controller types		$b_{K,\max}$ (N/mm)
State feedback controllers	LKF-SFC1	LKF without delayed feedback	≈ 500
	LKF-SFC2	LKF with delayed feedback	≈ 551
	LKF-SFC3	LKF with two-step optimization	≈ 880
	LQR-SFC	Robust LQR	≈ 262
Output feedback controllers	OFC1	Dynamic compliance minimization	≈ 275
	OFC2	Norm-bound treatment of delay	≈ 396
	OFC3	Padé approximation	≈ 551
	LKF-OFC	LKF delayed feedback	≈ 672
	PD	Base-level PD controller	≈ 180

ลิขสิทธิ์มหาวิทยาลัยเชียงใหม่
Copyright© by Chiang Mai University
All rights reserved

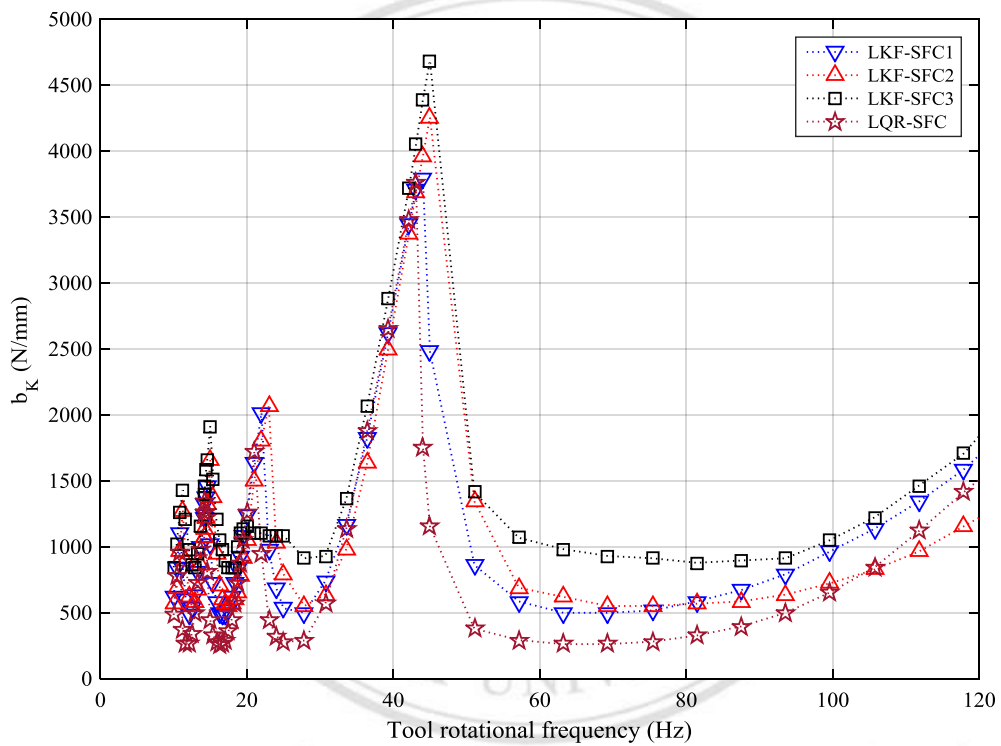


Figure 7.9 Test system SLD for the state feedback controllers

Copyright © by Chiang Mai University
All rights reserved

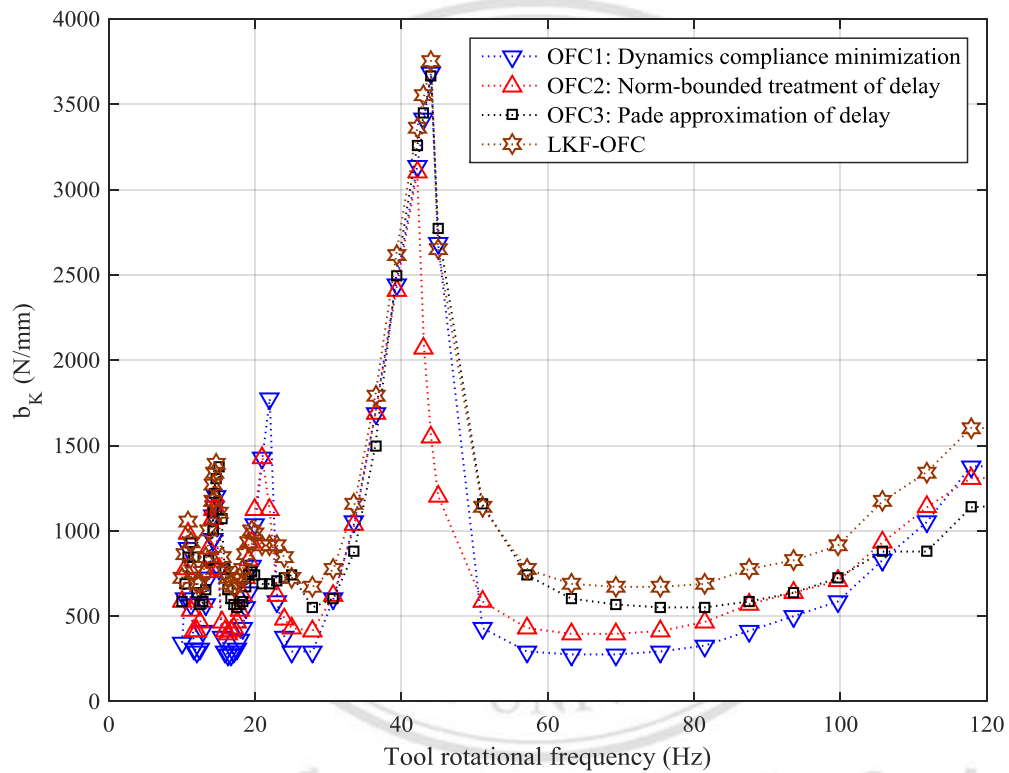


Figure 7.10 Test system SLD for the output feedback controllers

Copyright © by Chiang Mai University
All rights reserved

7.3 Cutting Emulations

Based on the cutting model (2.5), the cutting force at the tool tip was emulated by the actuator 2. The experimental test was performed with selected values for the depth-of-cut parameter ($b_K = bK_{cut}$). The experimental results are based on the eight controller designs which are the optimized state feedback controllers, LKF-SFC1-3 and LQR-SFC and four types of the optimized output feedback controllers OFC1-3 and LKF-OFC. The zero-vibration cutting force and the number of teeth in all simulations are the same as those used in the case with local PD control as shown in Figure 4.17. The rotational frequency of 16 Hz was used for state feedback controller and of 17 Hz for output feedback controller. The higher rotational speed was chosen so that the stability boundary can be seen clearly. The detailed plot of the stability boundaries closed to the operating points are shown in Figure 7.11 and Figure 7.16.

The time series data for the cutting emulations are shown in Figure 7.12 to Figure 7.15 for state feedback controller and Figure 7.17 to Figure 7.20 for output feedback controller.

The test were carried out with sequential step increases in the depth-of-cut parameter b_K . The values of each step were chosen depending on the cutting stability boundary of each controller at the predetermined testing rotational speed. Note that the value of b_K affects h_m as well as the feedback dynamics due to cutting, therefore the level of stable vibration increases with each step increase in b_K . The onset of instability is consistent with the experimental stability lobe diagrams and is indicated by an exponential growth in cutting vibration. The experiments were halted shortly after the onset of instability to prevent damage to the test system. It can also be observed that the control force levels are similar for all controllers even though the stability boundaries are quite different.

It can be seen that the levels of tool vibration for each value of b_K during stable cutting are similar for all the controllers. However, the peak magnitude of the control force u for output feedback control law (OFC) is less than those for the state feedback control law (SFC). This might be caused from the noise amplification effect from using digital differentiation to obtain velocity signal in the state feedback controllers and

noise attenuation property of the dynamic compensator in the output feedback controllers.

In summary, the maximum improvements of the cutting stability boundary for the state feedback controller and output feedback controller occur in LKF-SFC3 and LKF-OFC respectively. LKF-SFC3 can achieve a higher value of $b_{K,\max}$ than LKF-OFC but the magnitude of the control force in LKF-SFC3 is also higher. Also, the noise level in the OFC is lower than those in SFC.



ลิขสิทธิ์มหาวิทยาลัยเชียงใหม่
Copyright© by Chiang Mai University
All rights reserved

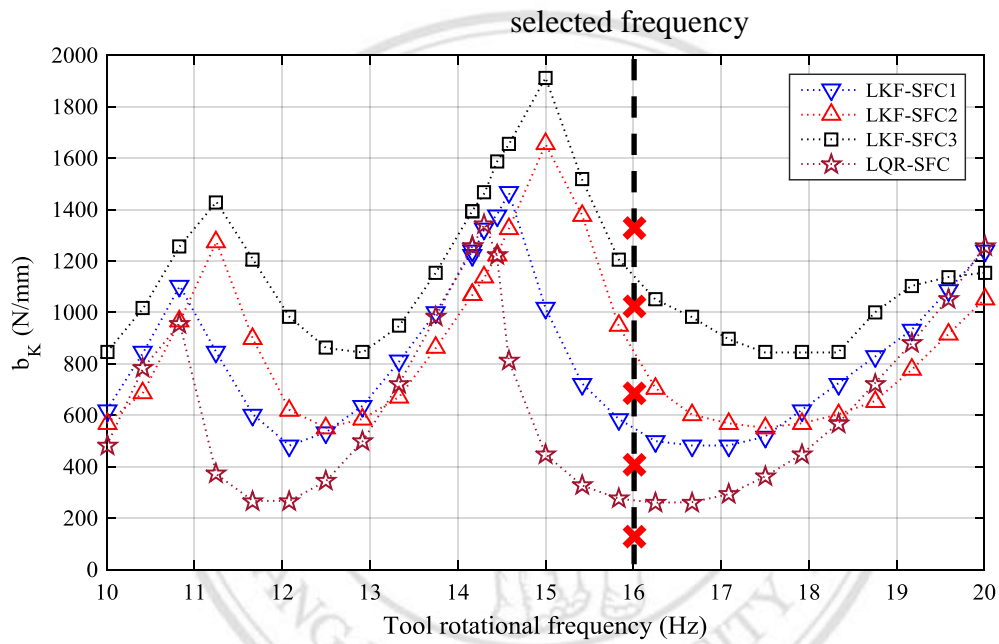


Figure 7.11 Close-up of experimental stability boundaries showing rotation frequency selected for cutting simulations based on Figure 7.9

ลิขสิทธิ์มหาวิทยาลัยเชียงใหม่
 Copyright© by Chiang Mai University
 All rights reserved

LKF-SFC1

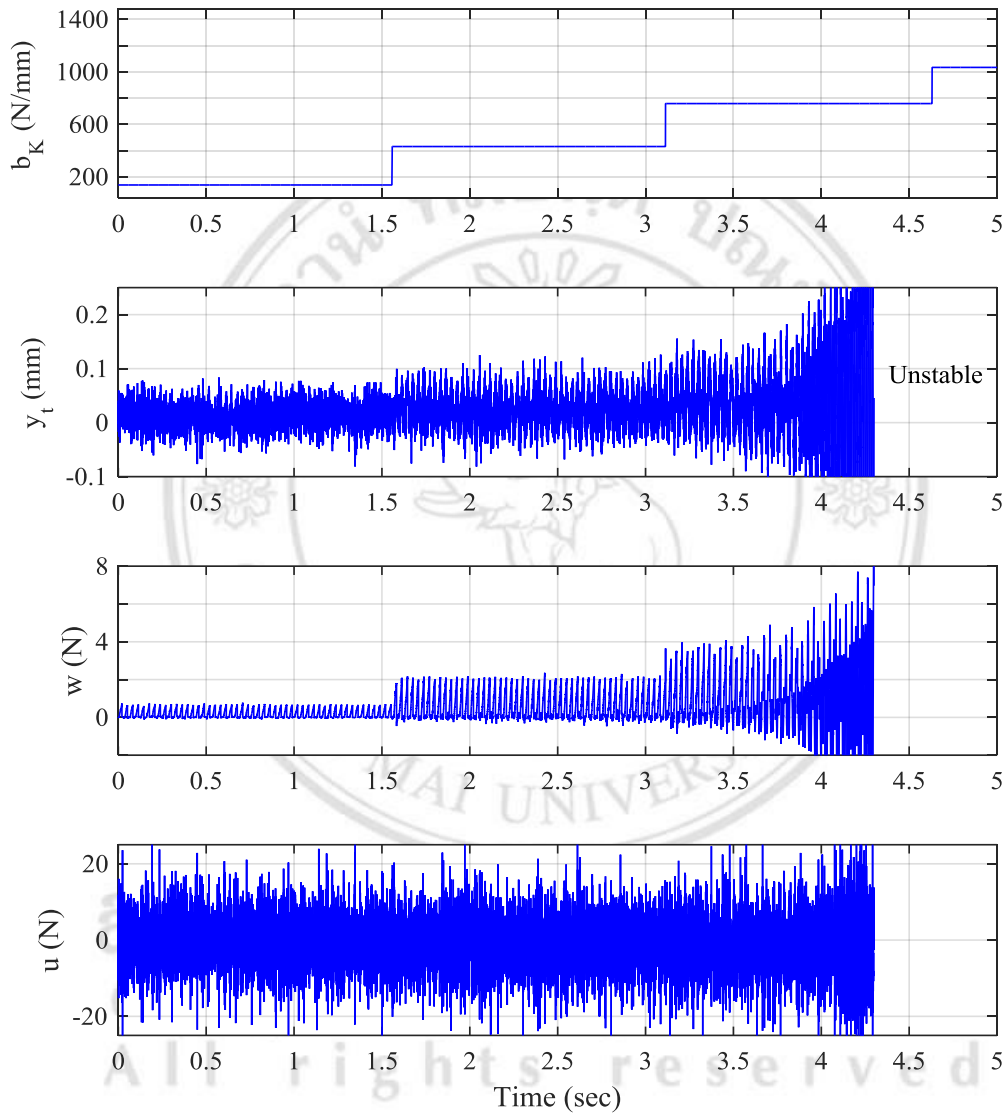


Figure 7.12 Cutting emulation on test system of LKF-SFC1 for 16 Hz rotational frequency

LKF-SFC2

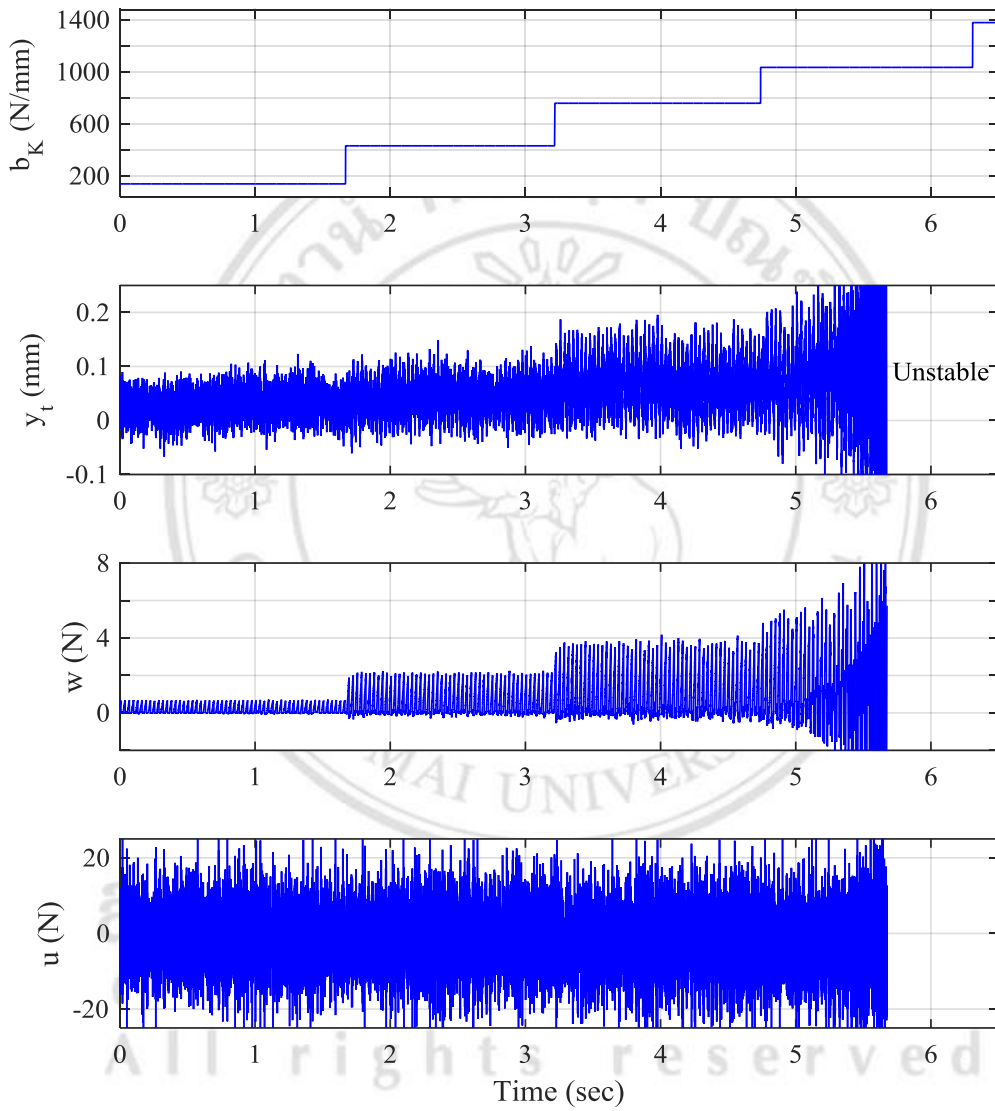


Figure 7.13 Cutting emulation on test system of LKF-SFC2 for 16 Hz rotational frequency

LKF-SFC3

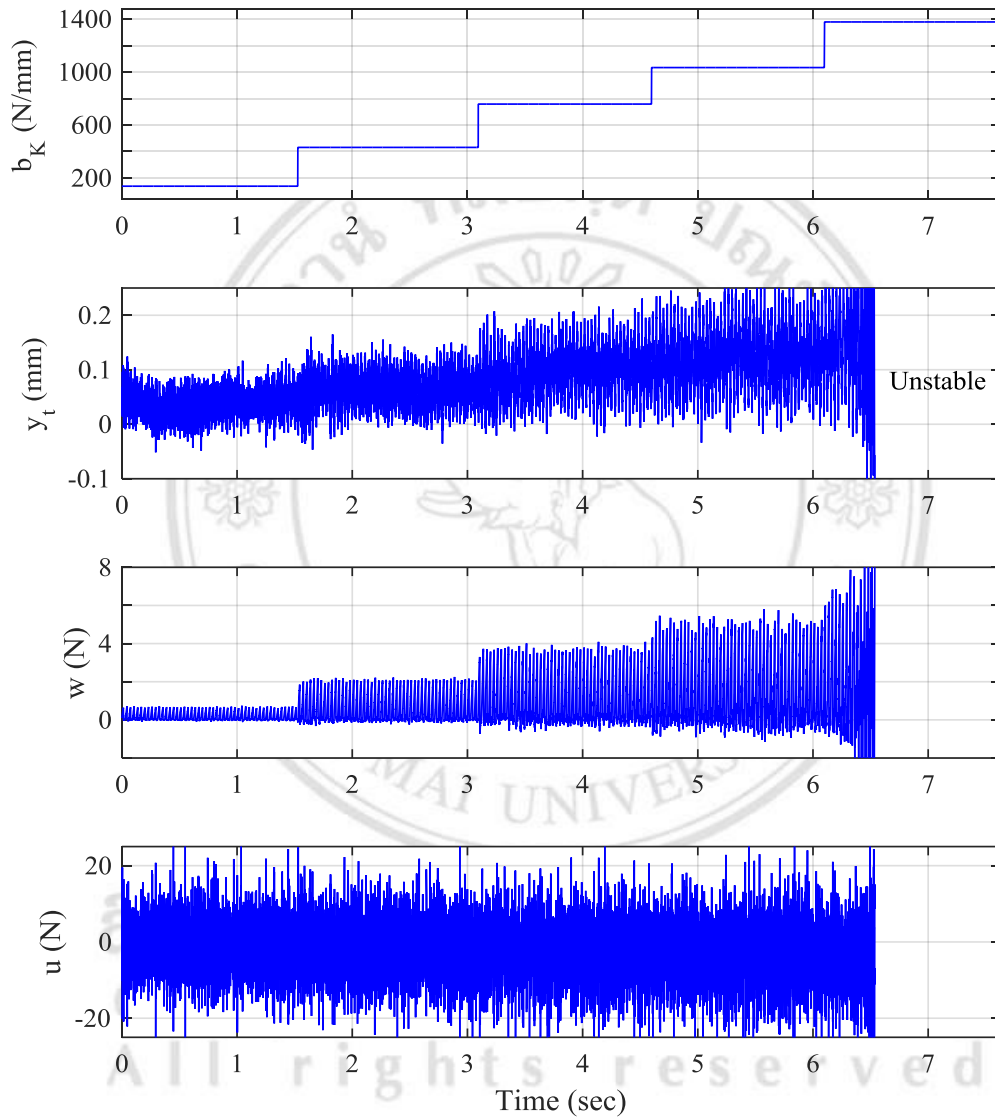


Figure 7.14 Cutting emulation on test system of LKF-SFC3 for 16 Hz rotational frequency

LQR-SFC

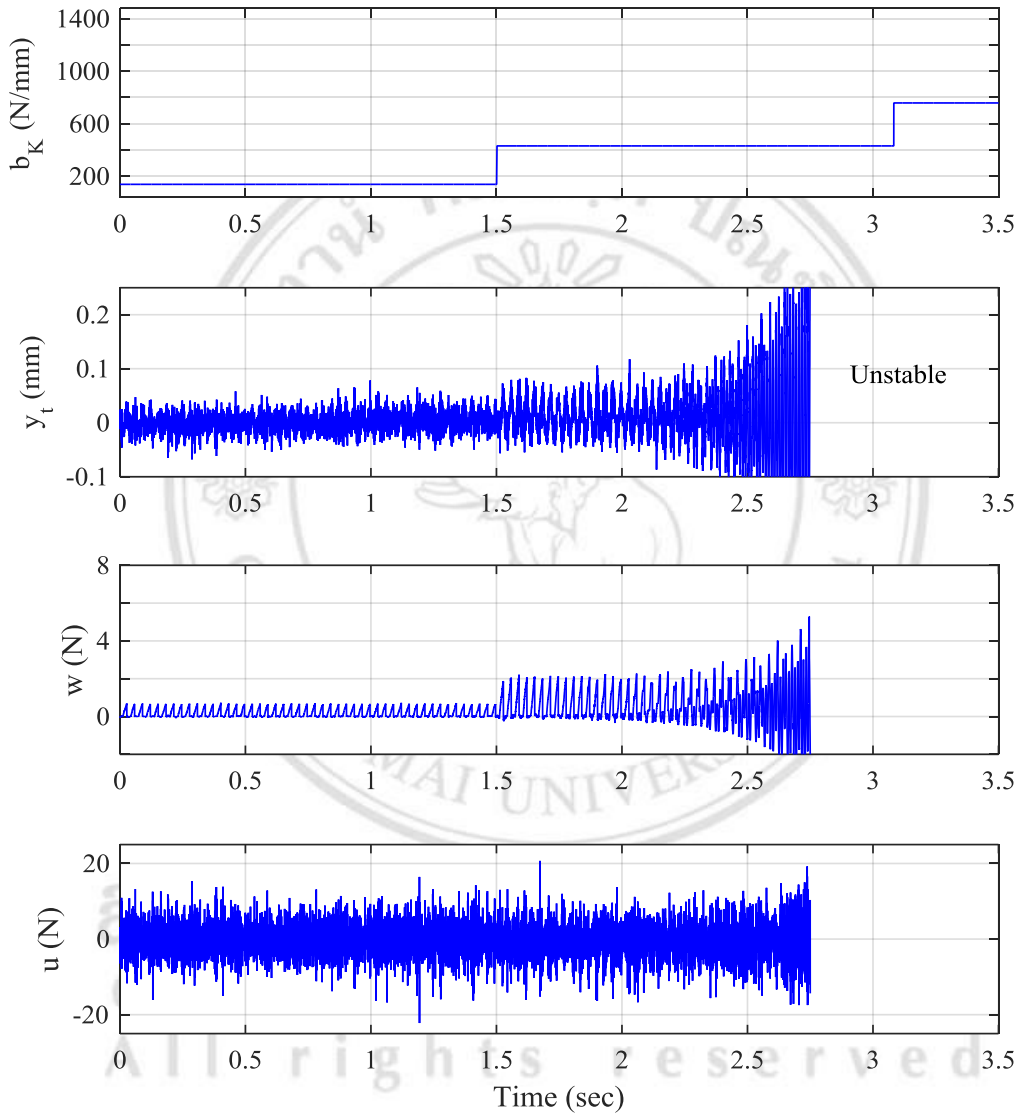


Figure 7.15 Cutting emulation on test system of LQR-SFC for 16 Hz rotational frequency

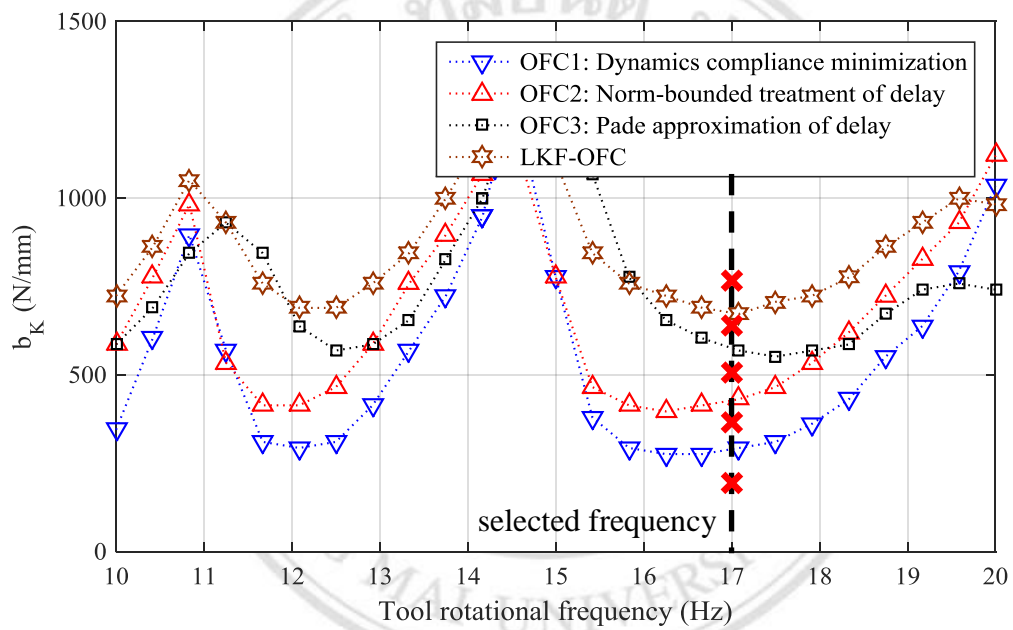


Figure 7.16 Close-up of experimental stability boundaries showing rotation frequency selected for cutting simulations based on Figure 7.10

Copyright© by Chiang Mai University
All rights reserved

OFC1: Dynamics compliance minimization

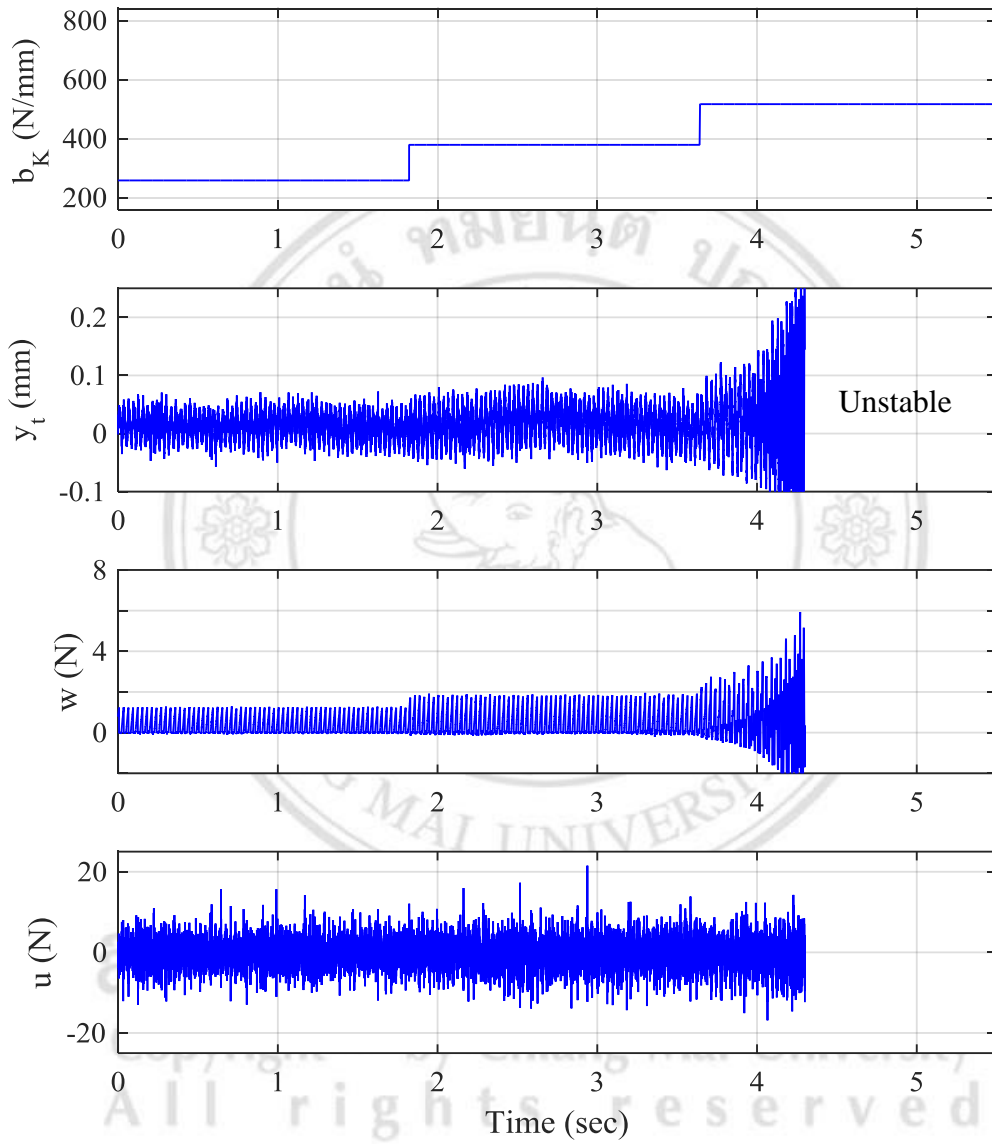


Figure 7.17 Cutting emulation on test system of OFC1 for 17 Hz rotational frequency

OFC2: Norm-bounded treatment of delay

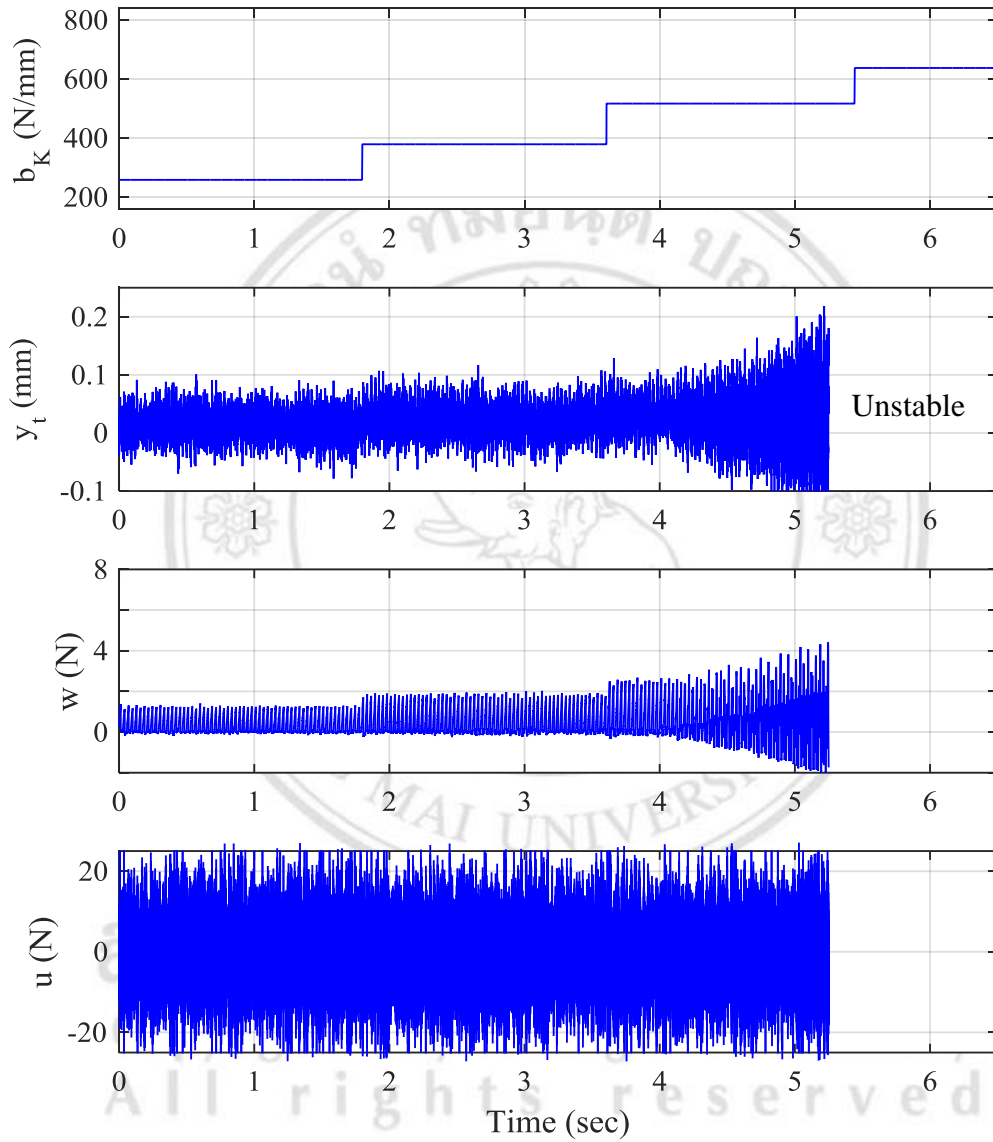


Figure 7.18 Cutting emulation on test system of OFC2 for 17 Hz rotational frequency

OFC3: Padé approximation of delay

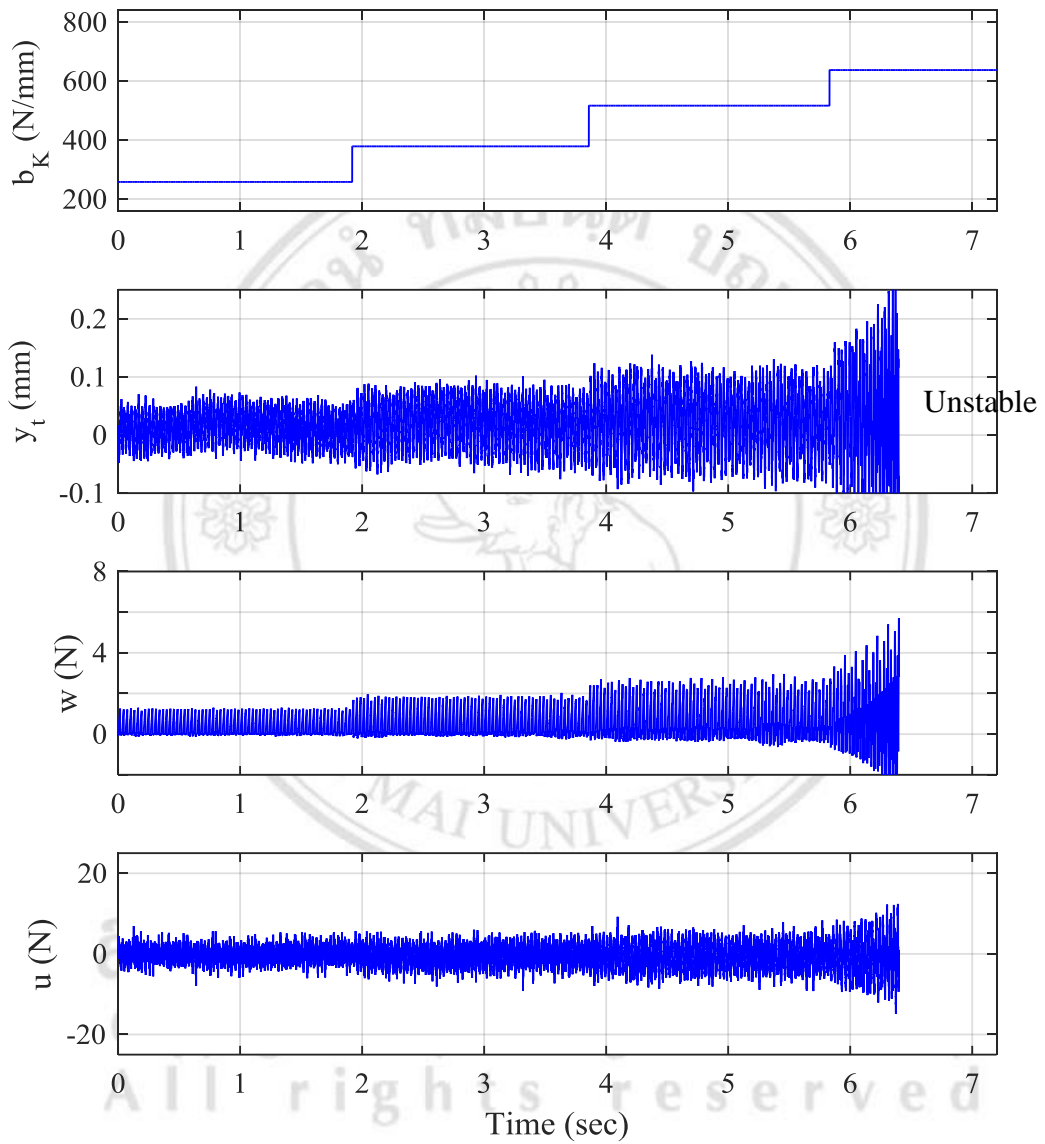


Figure 7.19 Cutting emulation on test system of OFC3 for 17 Hz rotational frequency

LKF-OFC

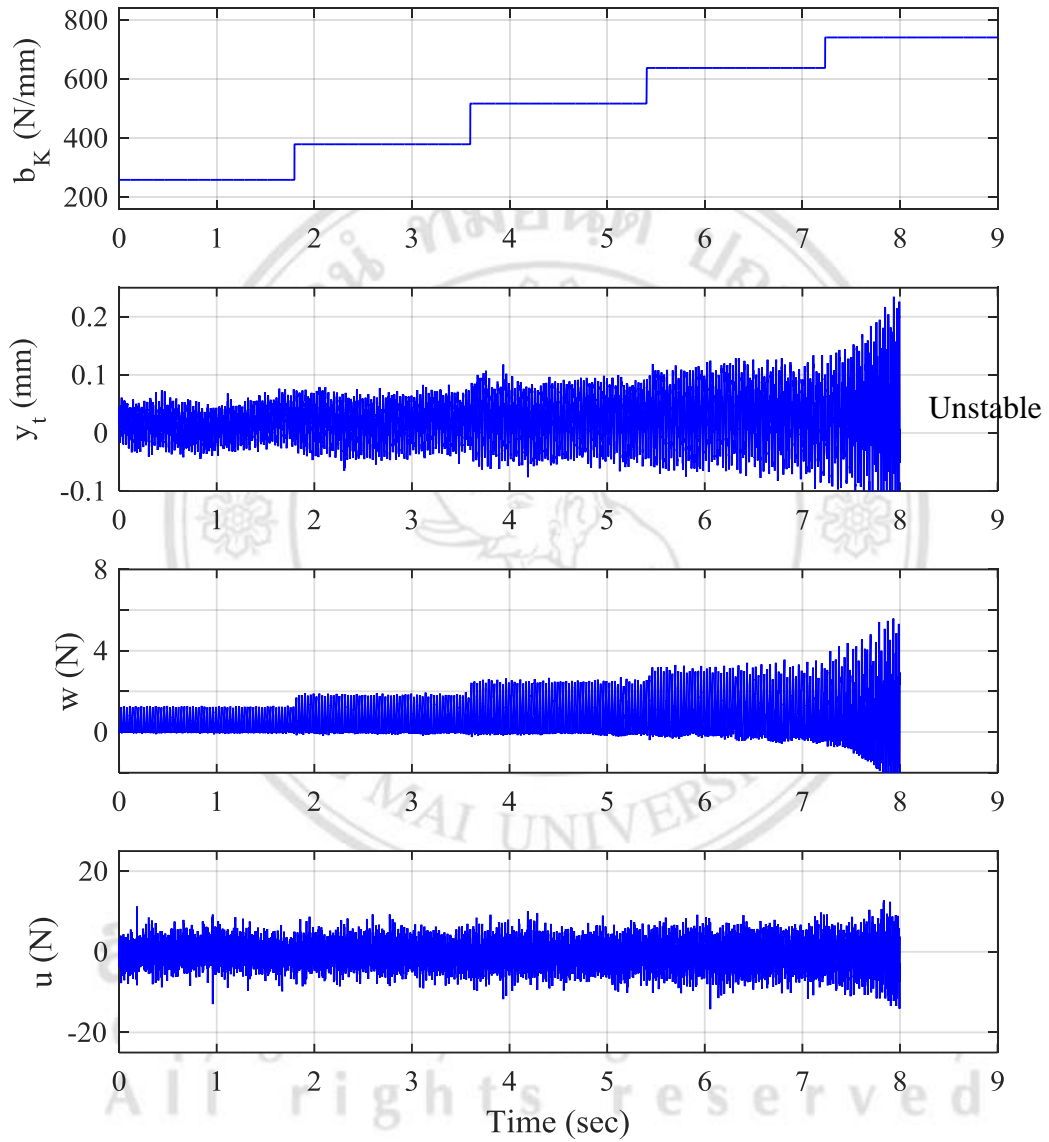


Figure 7.20 Cutting emulation on test system of LKF-OFC for 17 Hz rotational frequency



ลิขสิทธิ์มหาวิทยาลัยเชียงใหม่
Copyright© by Chiang Mai University
All rights reserved